Inhibition of RhoA pathway rescues the endocytosis defects in Oligophrenin1 mouse model of mental retardation

Malik Khelfaoui[1,2], Alice Pavlowsky[1,2], Andrew D. Powell[3], Pamela Valnegri[4], Kenneth W. Cheong[3], Yann Blandin[1,2], Maria Passafaro[4], John G.R. Jefferys[3], Jamel Chelly[1,2] and Pierre Billuart[1,2,*]

[1]Institut Cochin, Université Paris Descartes, CNRS UMR8104, 24 rue du Faubourg Saint Jacques 75014, Paris, France, [2]INSERM U567, 22 rue Méchain 75014, Paris, France, [3]School of Clinical and Experimental Medicine (Neuroscience), The Medical School, University of Birmingham, Edgbaston, Birmingham B15 2TT, UK and [4]DTI- CNR Institute of Neuroscience, 32 via Vanvitelli 20129, Milano, Italy

The patho-physiological hypothesis of mental retardation caused by the deficiency of the RhoGAP Oligophrenin1 (OPHN1), relies on the well-known functions of Rho GTPases on neuronal morphology, i.e. dendritic spine structure. Here, we describe a new function of this Bin/Amphiphysin/Rvs domain containing protein in the control of clathrin-mediated endocytosis (CME). Through interactions with Src homology 3 domain containing proteins involved in CME, OPHN1 is concentrated to endocytic sites where it down-regulates the RhoA/ROCK signaling pathway and represses the inhibitory function of ROCK on endocytosis. Indeed disruption of *Ophn1* in mice reduces the endocytosis of synaptic vesicles and the post-synaptic α-amino-3-hydroxy-5-methylisoazol-4-propionate (AMPA) receptor internalization, resulting in almost a complete loss of long-term depression in the hippocampus. Finally, pharmacological inhibition of this pathway by ROCK inhibitors fully rescued not only the CME deficit in OPHN1 null cells but also synaptic plasticity in the hippocampus from *Ophn1* null model. Altogether, we uncovered a new patho-physiological mechanism for intellectual disabilities associated to mutations in RhoGTPases linked genes and also opened new directions for therapeutic approaches of congenital mental retardation.

INTRODUCTION

X-linked mental retardation (XLMR) is a genetic disease affecting mostly males. It is characterized by global cognitive impairment and an intelligence quotient below 70 (1). To date, 82 genes have been implicated in XLMR, which display a variety of clinical features. Traditionally, XLMR syndromes have been characterized as either syndromic or non-syndromic dependent on associated clinical abnormalities. Recent clinical re-evaluation of some XLMR cases has, however, suggested that the distinction may not be so clear-cut (2). The distinction between syndromic or non-specific forms of MR is somehow

vanishing and some MR cases have been reconsidered after clinical re-evaluation of patients. For example, the non-specific MR gene mental retardation associated with null mutations in *Oligophrenin1* (*OPHN1*) was originally described as non-syndromic (3), but later investigations suggested a syndromic XLMR associated with cerebellar hypoplasia and ventricular dilatation (4–6). We have recently reported that the *Ophn1* gene loss of function in mouse displays similarities to the human pathology, apart from the cerebellar hypoplasia, results in dendritic spine immaturity and in altered pre-synaptic function with a reduction of paired-pulse facilitation in CA1 hippocampus (7). These defects may

*To whom correspondence should be addressed. Tel: +33 144412481; Fax: +33 144412421; Email: pierre.billuart@inserm.fr or malik.khelfaoui@inserm.fr
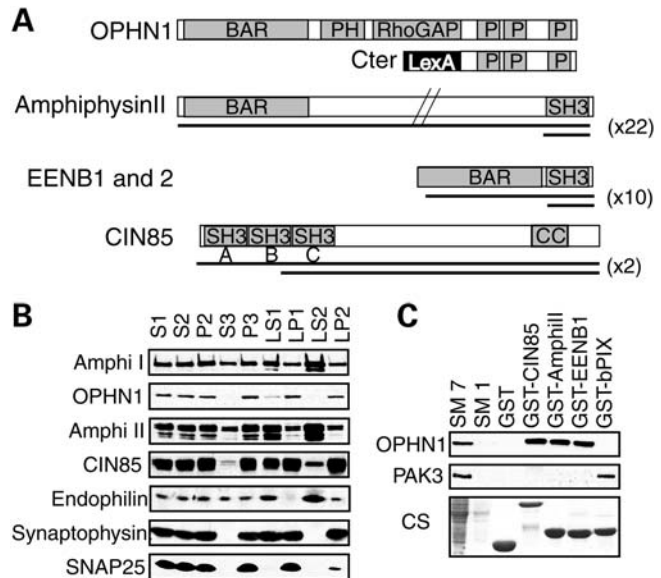
contribute to the spatial learning impairment in the animal model and presumably to the cognitive deficit in patients with mutations in the *Oligophrenin1* gene. However, the function of OPHN1 and its possible involvement in a pathway regulating synaptic transmission is still largely unexplored; as is the question whether the observed alterations in dendritic spine morphology are a cause or consequence of abnormal neurotransmission and/or synaptic activity (8,9).

In this study, we searched for new functions of OPHN1 using a biochemical approach and found that it interacts with molecules involved in clathrin-mediated endocytosis (CME). We next investigated this new function by studying the mouse model of *Ophn1* deficiency and found that various cellular mechanisms mediated through CME are impaired in the mutant. At the synapse, OPHN1 loss of function reduces both the synaptic vesicle and α-amino-3-hydroxy-5-methylisoazol-4-propionate (AMPA) receptor endocytosis affecting synaptic plasticity. Finally, we showed that the RhoA/ROCK signaling pathway is up-regulated in *Ophn1* knock-out cells and that pharmacological inhibition of this pathway restores not only the CME deficits, but also the proper synaptic plasticity in *Ophn1* mouse model. In addition, these results highlight new patho-physiological mechanisms for intellectual disabilities associated to mutations in RhoGTPases linked genes.

RESULTS

OPHN1 interacts with three molecules involved in CME: amphiphysins, endophilins and CIN85

Apart from the central RhoGAP domain, OPHN1 contains an N-terminal Bin/Amphiphysin/Rvs (BAR) (10) domain followed by a Pleckstrin homology domain and a C-terminal domain with three proline-rich regions at amino acid positions 575, 629 and 740 with multiple Src homology 3 (SH3) binding domains (Fig. 1A) (3,11). Using this latter region as bait in the two-hybrid system, we screened a cDNA library from fetal brain and found that amphiphysin II (12), endophilin EENB1 and B2 proteins (13) and CIN85 (14) interact with OPHN1 (Fig. 1A). As these proteins are known to participate in different steps of CME (15–17), we explored this new putative function of OPHN1. Previous studies have shown that all four proteins are expressed in cortical neurons at synaptophysin-positive synapses (11,15,18–22). We then performed fractionation experiments in rat adult brain to test whether OPHN1 is enriched in the same fractions as amphiphysin I or II, Cin85 and endophilin. We found that the distribution profile of OPHN1 in the pellet fractions is similar to Cin85 and synaptophysin, a pre-synaptic protein attached to synaptic vesicle membranes (Fig. 1B). As amphiphysin I and II and endophilin were more enriched in the supernatant fractions and only partially distributed with OPHN1, suggests that their interactions with OPHN1 may not be constitutive but regulated during endocytosis. We also investigated the consequences of the loss of OPHN1 function on the expression or fractionation pattern of these OPHN1-interacting proteins using protein brain extract from *Ophn1* null mice (*Ophn1*$^{-/y}$) and found that they were not altered compared with their wild-type littermates (*Ophn1*$^{+/y}$) (data not shown). We next used glutathione S-transferase (GST) pull-

Figure 1. OPHN1 protein interactions with amphiphysins, endophilins and CIN85. (**A**) Two-hybrid results from OPHN1 screening using the C-terminal end (LexA-Cter). Black bars show overlapping cDNA clones recovered from the two-hybrid screening (x): number of independent clones recovered from the screening; in all cases, they include at least one SH3 site. BAR: Bin/amphiphysin/Rvs, PH: Pleckstrin Homology, RhoGAP: Rho GTPase activating protein, CC: coiled–coiled, P: proline-rich domains. (**B**) Rat brain fractionation experiments showing the distribution of OPHN1 together with its binding partners, amphiphysin I and II (Amphi I and II), CIN85 and endophilin. Synaptophysin and SNAP25 were used as positive control of fractionation. Fractions as follows: S1, post-nuclear/cell soma; S2, supernatant; P2, mitochondria and crude synaptosomes; S3, cytosolic; P3, microsomal/light membrane compartment; LS1, soluble lysate; LP1, synaptosomal/presynaptic plasma membrane; LS2, synaptosolic; LP2, enriched in SV and pre-synaptic plasma membranes. (**C**) GST pull-down experiments. Purified GST-SH3 domains of CIN85 (ABC), amphiphysinII (AmphiII) or endophilin (EENB1), but not the one from βPIX, are able to strongly bind to OPHN1 protein. Starting material (SM): protein extract at either 1 mg/ml (SM1) or 7 mg/ml (SM7). A 1 mg of protein extract was used for each pull-down experiment; CS: Coomassie staining of SDS–PAGE gel is presented as loading control.

down experiments to confirm and study the OPHN1 interactions. The SH3 domains of CIN85, amphiphysin II and EEN-B1 were able to retain endogenous OPHN1 from adult mouse brain extracts, whereas neither GST alone nor GST-SH3 domain of βPIX, a Rac/Cdc42 exchange factor known to interact with PAK3 (23), were able to bind to OPHN1 (Fig. 1C). These results not only confirmed the interactions but also showed the specificity of the SH3–proline-rich domain interactions between OPHN1 and its partners. Amino acid-sequence analyses of proline-rich motifs in OPHN1 revealed the presence of two putative binding sites for amphiphysin II (P/IXRPXR) at position 575 and 740, one CIN85 binding site (PXXXPR) at position 575 and one endophilin binding site (PPXRP) at position 740 (24,25). In order to discriminate between the different proline-rich binding sites of OPHN1, we expressed three enhanced green fluorescent protein (EGFP)-fused proteins in COS cells corresponding to either the whole C-terminal domain of OPHN1 (Cter) or parts of it, Cter A and B (Supplementary Material, Fig. S1B) (11). Protein extracts from transfected COS cells were incubated with various GST-purified SH3 domains

from amphiphysin I and II, CIN85 (three SH3 sites ABC) and endophilins (EEN, EEN-B1 and EEN-B2) to test the relative affinity of each EGFP-fused constructs of OPHN1. We found that the first proline-rich region has overlapping binding sites for CIN85 and amphiphysin II and the third proline-rich region binds only endophilins (Fig. 1A and Supplementary Material, Fig. S1A). Among the different partners of OPHN1, amphiphysin I and II and endophilins contain only one SH3 binding site at their C-terminal end, whereas CIN85 has three N-terminal sites A, B and C (Fig. 1A and Supplementary Material, Fig. S1B). We tested *in vitro* various combinations of GST-fused SH3 sites of CIN85 (constructs A, B and C, Supplementary Material, Fig. S1B) for affinity to OPHN1 CterA protein and found that all three SH3 sites of CIN85 are potentially able to bind independently or in combination to the first proline-rich site of OPHN1 (Supplementary Material, Fig. S1B). Taken together, these data show that OPHN1 interacts with proteins implicated in CME via proline−SH3 binding sites and suggest that OPHN1 plays, through its interactions with these known adaptor molecules, a functional role at endocytic sites.

Loss of OPHN1 leads to the activation of the RhoA/ROCK signaling pathway and reduced receptor endocytosis in various cell types
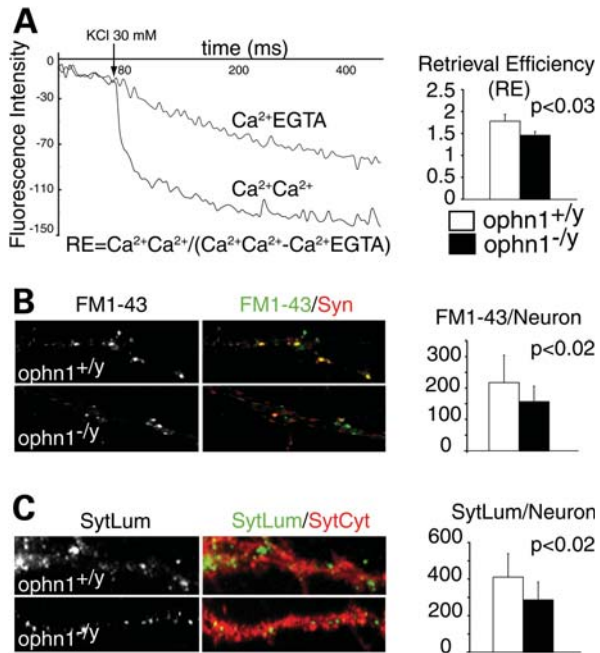
OPHN1 contains a central RhoGAP domain, which regulates the RhoA/ROCK pathway (11,18). As this pathway has been shown to modulate the receptors endocytosis through endophilin phosphorylation and interaction with CIN85 (26,27), we examined the level of its activation in $Ophn1^{-/y}$ cells. We first studied the activation kinetics of RhoA in serum-stimulated fibroblasts, which results in robust activation of RhoA. Using GST pull-down experiments, we found that total RhoA activity is approximately doubled in $Ophn1^{-/y}$ compared with $Ophn1^{+/y}$ (Supplementary Material, Fig. S2A). We next looked at the activity of the RhoA effector ROCK through quantification of phosphorylation status of one of its substrate, the myosin-binding subunit (MYPT1) of the myosin phosphatase in astroglial cells (28). $Ophn1^{-/y}$ cells presented a significant increase of MYPT1 phosphorylation ($\times 1.4$) compared with $Ophn1^{+/y}$ (Supplementary Material, Fig. S2B; $Ophn1^{+/y}$: 0.45 ± 0.05; $Ophn1^{-/y}$: 0.64 ± 0.11; $P < 0.05$, Mann−Whitney test (MW), $n = 4$); a phenotype, which could be completely abolished by pre-incubation of the cells with the ROCK inhibitor Fasudil (Supplementary Material, Fig. S2B). These results demonstrated that loss of function of OPHN1 increases the activation of the RhoA/ROCK pathway.

To directly test the consequences of this activation on CME, we performed endocytic assays on primary astroglial cells from both genotypes using fluorescent-labeled transferrin (Tf) or epidermal growth factor (EGF) as tracer of constitutive or inducible CME of their respective receptors (Supplementary Material, Fig. S2C). Using FACS analysis, we found that $Ophn1^{-/y}$ cells have a reduced constitutive internalization rate (64%) compared with $Ophn1^{+/y}$ (Supplementary Material, Fig. S2C; $Ophn1^{+/y}$: 87 ± 11; $Ophn1^{-/y}$: 31 ± 4, $P < 0.01$ two-tailed Student's *t*-test $n = 4$). A similar decrease in EGF receptor internalization was observed in $Ophn1^{-/y}$ fibroblasts using cell-image analyses (data not shown). We next used

a specific inhibitor of ROCK, Y27632 (29) to test whether incubation of $Ophn1^{-/y}$ astroglial cells with this drug could abolish the CME deficit. Treatment with Y27632 did not significantly alter endocytosis in $Ophn1^{+/y}$ cells (Supplementary Material, Fig. S2C; $Ophn1^{+/y}$ (−)Y27632: 87 ± 11; $Ophn1^{+/y}$ (+)Y27632: 74 ± 7). This result confirms previous studies showing that ROCK inhibition has no effect on endocytosis in basal conditions (26,30). In contrast, treatment with Y27632 fully rescued the defect in $Ophn1^{-/y}$ cells (Supplementary Material, Fig. S2C; $Ophn1^{-/y}$ (−)Y27632: 31 ± 4; $Ophn1^{-/y}$ (+)Y27632: 84 ± 8; $P < 0.01$ two-tailed Student's *t*-test, $n = 4$). Thus the activation of the RhoA/ROCK signaling pathway secondary to OPHN1 loss of function is responsible for the reduction of CME in astroglial cells.

Synaptic vesicle endocytosis are reduced in cortical neurons

Since removal of amphiphysins from mouse brain led to some defects in the synaptic vesicles endocytosis (SVE) (31), we tested whether *Ophn1* null mice displayed a similar deficit. Using purified synaptosomes from $Ophn1^{+/y}$ and $Ophn1^{-/y}$ mice cortices, we compared the exocytotic and recycling efficiency of synaptic vesicles (SV). High potassium-evoked glutamate release was unaffected in $Ophn1^{-/y}$ synaptosomes (7.1 ± 0.6 versus 6.5 ± 2.1 nmol/mg, $P = 0.6$, two-tailed Student's *t*-test, $n = 3$). We next employed the fluorescent amphipathic styryl dye, FM2-10, to study the recycling of SV after two successive depolarization steps by high potassium concentration (32). Using Ca^{2+} or EGTA containing buffers for unloading steps, we calculated an index called retrieval efficiency (33) to allow direct comparison of recycling between genotypes (Fig. 2A, left panel). We found that the Ca^{2+}-dependant retrieval efficiency was decreased by 17% in $Ophn1^{-/y}$ (Fig. 2A, right panel, $Ophn1^{+/y}$: 1.82 ± 0.02; $Ophn1^{-/y}$: 1.42 ± 0.01; $P < 0.03$, two-tailed Student's *t*-test, $n = 4$). Since the release of glutamate was normal, we hypothesized that $Ophn1^{-/y}$ synapses would have a deficit in the synaptic vesicle endocytosis/recycling. We subsequently used a cellular model to study the uptake of another fluorescent amphipathic styryl dye, the FM1-43, in individual synapses from cortical neurons after potassium stimulation (34). Whereas there was no effect on synaptic density as measured by the density of the pre-synaptic marker synaptophysin ($Ophn1^{+/y}$: 385 ± 97; $Ophn1^{-/y}$: 402 ± 122; $P < 0.13$, MW test, $n = 3$), we found that loss of OPHN1 function reduces the density of FM1-43 puncta (−28%) co-localized with synaptophysin (Fig. 2B; $Ophn1^{+/y}$: 217 ± 95; $Ophn1^{-/y}$: 157 ± 56; $P < 0.02$, MW test, $n = 3$). We also analyzed the internalization of synaptotagmin1 as a marker of SV, which undergoes recycling between the pool of SV and pre-synaptic membranes during exocytosis and endocytosis (35). First we determined that the expression of synaptotagmin1 was not affected in $Ophn1^{-/y}$ and that it co-localized with the pre-synaptic markers vesicular glutamate transporter-1 (VGluT-1) during resting conditions (data not shown). We then quantified synaptotagmin1 antibody uptake in $Ophn1^{+/y}$ and $Ophn1^{-/y}$ neurons (Fig. 2C) after stimulation by high potassium and found that the number of synaptotagmin1 positive synapses is decreased in $Ophn1^{-/y}$ cells (−29%) confirming the FM1-43 results (Fig. 2C; $Ophn1^{+/y}$:
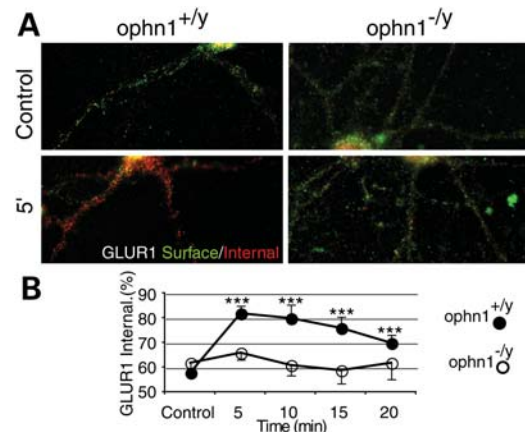
Figure 2. Reduced synaptic vesicle recycling and uptake in synaptosomes and neurons from $Ophn1^{-/y}$. (**A**) Decreases of fluorescence were measured from FM2-10-labeled synaptosomes using different unloading conditions of Ca^{2+} (Ca/Ca or Ca/EGTA). A ratio, called retrieval efficiency (RE) was calculated at 300 s for both genotypes. Synaptosomes from $Ophn1^{-/y}$ (RE=1.48 ± 0.06) showed a reduced RE (17%) compared with $Ophn1^{+/y}$ (RE = 1.78 ± 0.15) ($P = 0.03$, two-tailed Student's t-test, $n = 4$). (**B**) Neurons were stimulated by high potassium buffer in the presence of FM1-43 dye. Only FM1-43 punctae (in green) co-localized with the pre-synaptic protein synaptophysin (Syn, in red) were quantified (FM1-43+). $Ophn1^{-/y}$ neurons (157 ± 48) presented a 28% reduction in FM1-43 compared with $Ophn1^{+/y}$ (217 ± 86)($P <$ 0.02, Mann–Whitney test, $n = 3$). (**C**) For synaptotagmin1 antibody uptake experiments, neurons were stimulated in the presence of an antibody directed against the luminal domain (SytLum in green). The cells were fixed, permeabilized and stained with a second antibody against cytoplasmic domain (SytCyt in red). $Ophn1^{-/y}$ neurons (291 ± 92) presented a 29% reduction in synaptotagmin1 antibody uptake compared to $Ophn1^{+/y}$ (411 ± 127) ($P <$ 0.02, Mann–Whitney test, $n = 2$).

411 ± 127; $Ophn1^{-/y}$: 291 ± 92; $P < 0.02$, MW test, $n = 3$). In conclusion, we showed that loss of OPHN1 function reduces the uptake and internalization of various tracers in different models suggesting that OPHN1 contributes to the regulation of a pathway controlling synaptic vesicle endocytosis in a significant fraction of synapses.

Loss of OPHN1 affects AMPA receptor endocytosis and synaptic plasticity in the hippocampus

In addition to its localization in the pre-synaptic compartment, OPHN1 is also present at the post-synaptic site (7,11,18), where it could regulate the recycling of various receptors including the AMPA receptors (AMPARs) (36). Translocation of AMPARs from cell surface to intracellular compartments in $Ophn1^{+/y}$ and $Ophn1^{-/y}$ neurons was visualized and quantified by an 'antibody feeding' immunofluorescence internalization assay. In $Ophn1^{+/y}$ neurons, the basal endocytosis of GluR1 subunit was rapid, reaching a maximum degree in 5 min without reaching a plateau (Fig. 3A and B and Supplementary Material, Fig. S3). In contrast, in $Ophn1^{-/y}$ neurons, GluR1
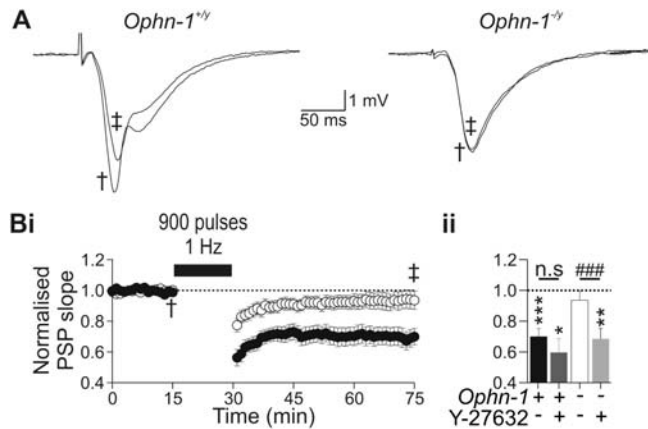

Figure 3. Reduced AMPA receptor endocytosis in $Ophn1^{-/y}$ ippocampal neurons endocytosis of GluR1 subunit was visualized and quantified by the immunofluorescence internalization assay as indicated. Pre-labeled AMPA receptors remaining on the surface are in green, internalized receptors in red (see Materials and Methods). Basal GluR1 subunit internalization at 5 min in $Ophn1^{+/y}$ and $Ophn1^{-/y}$ neurons is shown in (**A**). The quantitation of time course of basal GluR1 subunit internalization in $Ophn1^{+/y}$ and $Ophn1^{-/y}$ neurons, measured as the ratio of internalized (red)/total (red + green) fluorescence, normalized to control (total=100) is shown in (**B**). In $Ophn1^{-/y}$ neurons GluR1 subunit endocytosis was significantly down-regulated.

subunit endocytosis was significantly down-regulated (Fig. 3A and B and Supplementary Material, Fig. S3), suggesting that OPHN1 contributes in the mechanism controlling the AMPARs trafficking.

Interestingly, this effect was selective of GLUR1 subunit, since GLUR2 internalization rate was not affected by the loss of OPHN1 function (Supplementary Material, Fig. S3).

Current theories suggest that N-methyl-D-aspartic acid (NMDA)-dependent long-term depression (LTD) is a result of AMPAR internalization at the post-synaptic membrane (37,38) via CME (36,39,40). As $Ophn1^{-/y}$ mice display reduced AMPAR internalization in neurons, we hypothesized that LTD may be altered in $Ophn1^{-/y}$ mice. We therefore examined NMDA-dependent LTD at the CA3:CA1 synapse using the extracellular recording technique (Supplementary Material, Fig. S4Bi and Bii). Synaptic responses were recorded in the stratum radiatum of the CA1 region of the hippocampus, and were evoked by stimulation of the Schaffer collateral. Repetitive stimulation at low-frequency (900 pulses, 1 Hz) depressed synaptic responses in $Ophn1^{+/y}$ slices (0.70 ± 0.05, $n = 14$, $P < 0.001$, Fig. 4A and Bi), but not $Ophn1^{-/y}$ slices (0.94 ± 0.06, $n = 11$, $P = 0.66$, Fig. 4A and Bi). As the reduction in CME in $Ophn1^{-/y}$ astroglial cells was rescued by treatment with the Y27632 ROCK inhibitor (Fig. 3C), we examined whether the observed deficit in the NMDA-dependent LTD was similarly reversed. Y27632 (10 μM) was added to the circulating artificial cerebrospinal fluid (aCSF) for 25 min before, and throughout the LTD protocol and did not alter population synaptic potentials (PSP) amplitude (Supplementary Material, Fig. S4Ai and Aii). In Y27632-treated $Ophn1^{+/y}$ slices, low frequency repetitive stimulation produced LTD (0.62 ± 0.08, $n = 5$, $P < 0.01$, Fig. 4Bii), the magnitude of which did not differ from untreated slices ($P = 0.61$). In contrast, in $Ophn1^{-/y}$ slices, Y27632 revealed that repetitive stimulation

Figure 4. Long-term depression (LTD) is reduced in $Ophn1^{-/y}$ hippocampal slices. (**A**) Population synaptic responses recorded from the stratum radiatum of CA1, before (†) and after (‡) induction of LTD in $Ophn1^{+/y}$ (*left* panel) and $Ophn1^{-/y}$ slices (right panel). LTD was induced by repetitive stimulation (900 pulses, 1 Hz) of the Schaffer collaterals. (**B**i) LTD was reduced in $Ophn1^{-/y}$ slices (white circles) compared with $Ophn1^{+/y}$ slices (dark circles). Inhibition of ROCK by superfusion of Y-27632 (10 μM) resulted in LTD being observed in $Ophn1^{-/y}$ slices (**B**ii, light gray column), but did not alter expression of LTD in $Ophn1^{+/y}$ slices (**B**ii, dark gray column). The degree of induction of LTD was taken as the mean normalized PSP (population synaptic potential) slope between 40 and 45 min post-induction protocol. (**B**ii) To evaluate whether LTD was induced, a one sample Student's *t*-test was used (Null hypothesis value was 1. ***$P < 0.001$, **$P < 0.005$ and *$P < 0.01$). Comparisons between control and drug-treated slices were performed using an independent samples *t*-test (###$P < 0.001$). The significance value in all tests was set as 0.01, to allow for multiple comparisons.

induced LTD (0.64 ± 0.03, $n = 5$, $P < 0.005$, Fig. 4Bii), which significantly differed from untreated slices ($P < 0.001$). These data therefore support the hypothesis that OPHN1 may also function as a regulator of AMPAR internalization via a ROCK-dependent mechanism of CME.

DISCUSSION

Using biochemical and physiological approaches, we identified a new function of OPHN1 in CME through the regulation of Rho GTPase signaling pathways. F-actin bound OPHN1 (11) is recruited to endocytic sites by SH3−proline interactions with three known adaptor molecules involved in CME: endophilin, amphiphysin and CIN85. We have previously shown that the N-terminal end of OPHN1 containing the BAR domain negatively regulates the RhoGAP activity (11). Locally, the increase in OPHN1 concentration would favor its homo-dimerization and/or binding to curved membranes and its RhoGAP activity would be activated by either a change in its conformation or by an alternative unknown mechanism (41). Activated OPHN1 negatively regulates the RhoA/ROCK pathway, repressing the inhibition of this pathway on CME (Supplementary Material, Fig. S5). This effect could be direct through endophilin phosphorylation by ROCK and consecutive inhibition of CIN85 interaction with endophilin as shown by Kaneko *et al.* (26). As endophilin concentrates OPHN1 to endocytic sites, this would suggest the existence of a negative retrocontrol loop of endophilin on RhoA/ROCK inhibition. Alternatively or in combination with this mechanism, other activities of ROCK effectors

such as myosin light chain kinase (42) may be regulated to remodel the actin cytoskeleton during endocytosis.

At the synapse, the differences in synaptosome vesicle cycling between $Ophn1^{+/y}$ and $Ophn1^{-/y}$ suggest deficits in pre-synaptic function. In line with these findings, we previously showed that $Ophn1^{-/y}$ exhibits an impairment in paired-pulse facilitation measured in CA1 hippocampus that could result either from an increase of release probability, a reduction of build-up Ca^{2+} or a slower rate of SV recycling mechanism (7).

In addition to synaptosome and cellular studies using exogenous and endogenous tracers, impairment in SV cycling was reinforced by electrophysiological studies that showed are a deficit in the size of the pool of readily releasable vesicles together with slower vesicle recycling at the perforant path/dentate gyrus synapses (Powell *et al.*, submitted for publication). These synaptic transmission abnormalities in $Ophn1^{-/y}$ were also rescued by superfusion of hippocampal slices with Y27632 ROCK inhibitor (Powell *et al.*, submitted for publication).

Efficient recycling of SV is required to sustain the high-frequency synaptic transmission observed at synapses, and to maintain structural and functional integrity of the SV pools and presynaptic membrane compartments. Multiple mechanisms of SV recycling have been proposed (43). Direct endocytosis through a clathrin-mediated mechanism account for most of SV recycling under normal and sustained conditions as demonstrated recently by removal of clathrin which severely perturbed SVE in rodent CNS synapses (44).

The efficiency of the SV recycling machinery is important in the formation of a robust memory under challenging conditions. The different SV pools are required for efficient synaptic transmission and short-term memory formation and processing.

The *GDI1* gene, responsible in human for X-linked non-specific mental retardation, encodes α-GDI, a regulatory protein common to the Rab GTPases family. In mouse, lack of Rab-GDI perturbed the functionality of different SV pools at the presynaptic site. The reduction in SV did not alter long-term potentiation (LTP) following theta-burst tetanus in the CA1 region of the hippocampus but, as expected, was associated to a decrease in Post-tetanic-potentiation and a delayed recovery of synaptic transmission after depression (45).

In addition to its function in SVE, OPHN1 regulates the endocytosis of AMPARs at the post-synaptic site. Similarly to Arc/Arg3.1 (46,47), OPHN1 loss of function leads to a selective reduction of GLUR1 internalization, whereas the GLUR2 subunit is not affected. The AMPAR internalization experiments were performed in the absence of TTX (Tetrodotoxin). Therefore, in the used conditions of neuronal cell culture, the measured rates of AMPARs correspond to activity-dependant synaptic responses plus constitutive rate of internalization. Previous physiological studies (7) showed no difference in (S)-3,5-dihydroxyphenylglycine (DHPG)-induced LTD measured in CA1 hippocampus suggesting that mGluR-dependent AMPAR internalization is not affected by ophn1 loss of function. However, LFS-induced LTD, which is NMDA dependent, is severely impaired in OPHN1 KO. Altogether, these results from cellular and physiological studies suggest that activity-induced internalization of AMPAR is reduced in the ophn1 KO, affecting the GLUR1 subunit but not GLUR2. Previous studies have shown that in

mature hippocampal pyramidal cells, AMPARs occur predominantly as complexes containing GluR1/2 or GluR2/3 (48). The current model of AMPAR trafficking suggests that AMPARs containing GluR1 are inserted into synapses in an activity-dependent manner, whereas GluR2/3 heteromers cycle constitutively into and out of synapses (49). Since both subunits are internalized through CME, this would suggest that either OPHN1 controls the selective endocytosis of GLUR1 homomers or loss of OPHN1 function leads to secondary changes of the AMPAR subunit composition with a shift toward more GLUR2-lacking AMPARs. Alternatively, the selectivity for a pool of AMPAR may depend on the rate at which the receptors cycle into and out of the synapse (50).

What could be the physiological consequences of these changes? We have previously reported that LTP and mGLUR1-dependant LTD were not modified in the $Ophn1^{-/y}$ hippocampus (7). Here we found that NMDAR-dependant LTD is barely induced by low-frequency stimulation. Although both forms of LTD are mediated by the endocytosis of AMPAR, the signaling cascades that support each LTD are distinct. For instance, DHPG (mGLUR1 agonist)-stimulated LTD involved the local synthesis of Arc/Arg3.1 protein that binds to endophilins and dynamin, promoting AMPAR endocytosis (51,52). We can speculate that either OPHN1 is not involved in the cascade mediating mGLUR1-LTD or that Arc/Arg3.1 compensate for OPHN1 deficiency for this specific form of LTD.

Taken together, these compelling results suggest that part of the intellectual disability in *OPHN1* patients is a consequence of abnormal synaptic transmission linked to enhanced RhoA/ROCK activation and reduced endocytosis. Thus it might be possible to correct this deficit by reducing Rho GTPase signaling via inhibition of Rho-kinases. Consistent with this possibility, we found that blockade of Rho-kinases using the selective antagonist Y27632 could not only correct the decreased CME in cultured cells from $Ophn1^{-/y}$ mice, but also restore synaptic transmission and plasticity in $Ophn1^{-/y}$ hippocampal neurons. An exciting implication of this discovery is that drugs targeting Rho-kinases or others Rho GTPases effectors might be therapeutically useful for Rho GTPases linked mental retardations, assuming that they share a common patho-physiological mechanism.

MATERIALS AND METHODS

Primary cell culture and animals

Experimental procedures were performed in accordance with the European Communities Council Directive (86/809/EEC) regarding the care and use of animals and were approved by the local Ethics Committee. Cortical neurons, fibroblasts and astroglial cells from *Ophn1* knock-out animals and wild-type controls in C57BL/6 background were prepared by standard procedures as previously described (7).

Two-hybrid screening

A fetal brain matchmaker cDNA library (Cat# HL4028AH, lot# 7110056 from Clontech CA, USA) was screened with a bait consisting of the human *OPHN1* cDNA *Bgl*II/*Sal*I

fragment (amino acid 563–802) in VJL9 vector derived from pBTM116 (LexA binding domain); the yeast strain L40 (53) was maintained according to standard protocols (54). Out of 50 recovered cDNA clones from 1 million screened, 22 corresponded to amphiphysin II, 10 clones to endophilin genes (EEN-B1 and B2), and two clones to CIN85 protein.

GST pull-down

GST-tagged SH3 proteins were expressed in BL21 bacterial cells (Promega, WI, USA) and affinity purified according to standard protocols (55). Cos-1 cells were transfected using Lipofectamine (Invitrogen, CA, USA) with the following constructs: GFP-Cter, *Bgl*II/*Sal*I (amino acid 563–802) in pEGFP-CD11 (Clontech),GFP-Cter A *Bgl*II/*Pst*I (amino acid 563–677) in pEGFP-CD11,GFP-Cter B *Pst*I/*Sal*I (amino acid 677–802) in pEGFP-C3 (Clontech). Transfected proteins were detected with anti-GFP monoclonal antibody.

RhoA and ROCK activation assay

RhoA activation assay was performed starting from fibroblasts cell extracts according to manufacturer's instructions (Cytoskeleton, CO, USA).

Rho-kinase activity was quantified by MYPT1 phosphorylation on Thr-853 by western blot analyses starting from astroglial cells protein extracts. The ratio of phospho-MYPT1 against total MYPT1 density was calculated after quantification using densitometric analysis with ImageJ software.

Brain fractionation and preparation of synaptosomes

Rat brain from one adult male was processed according to protocols from (56), 75 μg of proteins were loaded on 5–15% gradient SDS–PAGE gel for western blot experiment. Synaptosomes from five to seven cerebral cortices of adult mice were prepared by centrifugation on discontinuous percoll gradients as previously described (32,57).

Glutamate exocytosis and content

The glutamate release was performed by enzymatic assay using the glutamate dehydrogenase as previously described using 1 mg of purified synaptosomes (58). The total glutamate content of 0.5 mg purified synaptosomes was determined after complete lysis and extraction in 0.1% Triton by the same method described above. The fluorescence intensities were acquired using a thermostated Cary Eclipse fluorescence spectrophotometer (Varian, CA, USA).

Synaptosome FM2-10 recycling

Two milligram of purified synaptosomes was loaded at $37°C$ with 100 μM FM2-10 (Molecular Probes, OR, USA) by depolarization with 30 mM KCl for 90 s in the presence of 1.3 mM Ca^{2+} as previously described (32,57). After two washes in low K+ saline solution with 1 mg/ml BSA, 1 mg of labeled synaptosomes were unloaded by a second 30 mM KCl induced depolarization in the presence of 1.3 mM Ca^{2+}

or 2 mM EGTA. Depending of the presence of Ca^{2+} ($Ca^{2+}\underline{Ca}^{2+}$ or $Ca^{2+}\underline{EGTA}$), we obtained two values of fluorescence that allowed us to calculate an index called retrieval efficiency [RE = CaCa/(CaCa–CaEGTA)] (33). By dividing the amount of endocytosis by exocytosis, this ratio bypasses the variability linked to synaptosomal purification and allowed us to quantitatively compare independent preparations from both genotypes.

FM1-43 uptake in cultured neurons

Synapses from individual cortical neurons were labeled with FM1-43 (Molecular Probes) according to Mozhayeva *et al*. (59). Neurons were then washed in a Tyrode buffer for 10 min and fixed in 4% paraformaldehyde/0.2% glutaraldehyde in PBS for 10 min. After fixation, cells were incubated with VGluT-1 or synaptophysin antibodies for detection of all synapses. Thirty-five neurons from each genotype were acquired with identical imaging conditions and analyzed similarly. Analyses were performed by quantification of the number of FM1-43 punctae co-localized with synaptophysin and normalized to the neuron surface. The experiment was repeated three times with similar results.

Synaptotagmin uptake in cultured neurons

Endocytosis of synaptotagmin1 antibody at steady state or after potassium-induced exocytosis was tested according to Takei *et al*. (35). Briefly, neurons were incubated at 37°C for 30 min with SytLum–Abs (SynSyst antibody) mouse monoclonal antibody, directed to the luminal domain of synaptotagmin and stimulated with 90 mM KCl for 2 min. Neurons were then washed and fixed before staining for synaptotagmin cytoplasmic domain antibody (SynSyst), rabbit polyclonal antibody to visualize the total of synaptotagmin vesicles pool. Twenty neurons from each genotype were acquired with identical imaging conditions and analyzed similarly. Positive synapses for SytLum antibody were normalized to the neuron surface. The experiment was repeated twice with similar results.

EGF and Tf uptake

Receptor-mediated endocytosis was analyzed by assays for EGF and Tf uptake as previously described (60). Adherent cells (fibroblasts or astroglial) were incubated with 15 µg/ml FITC-labeled Tf for 10 min at 37°C. Labeled cells were washed and re-suspended in medium after trypsin application and immediately put on ice for FACS analysis.

For rescue assays, cells were serum starved during 2 h in presence of 10 µM Y27632 (Sigma, MO, USA) (29) before incubation with labeled transferring. Flow cytometry measurements of at least 5000–10 000 cells per sample were analyzed using Cellquest software on a FACSCalibur (BD Biosciences, CA, USA). Fluorescent values from untreated $Ophn1^{+/y}$ are set to 100 and other conditions are expressed as percentage of Tf receptor uptake normalized to untreated $Ophn1^{+/y}$.

AMPAR internalization assay

Live hippocampal neurons at 15–18 days *in vitro* were labeled for 10 min at 37°C with an antibody directed against the extracellular region of either GluR1 or GluR2. After washing in PBS, 1 mM $MgCl_2$ and 0.1 mM $CaCl_2$ (PBS+MC), neurons were incubated at 37°C in conditioned growth medium for different times (0, 5, 10, 15, 20 min). Neurons were fixed for 5 min at room temperature in 4% paraformaldehyde/4% sucrose without permeabilization, and stained with FITC conjugated secondary antibodies for 1 h at room temperature, to visualize pre-labeled surface receptors. Neurons were then permeabilized for 1 min in 100% methanol at −20°C and stained with Cy3-conjugated secondary antibodies for 1 h at room temperature in GDB buffer (permeabilizing conditions: 30 mM phosphate buffer pH 7.4 containing 0.2% gelatin, 0.5% Triton X-100 and 0.8 M NaCl), to visualize pre-labeled internalized receptors. Red fluorescence average intensities indicative of internalization were divided by total average (red + green) fluorescence intensities to control (time 0) for synaptic density.

Image acquisition and analysis

Fluorescence images were acquired using a coolSnap digital camera (Roper Scientific) or a Photometrics CCD camera (Princeton Instruments, Trenton, NJ, USA). Acquired image sequences were saved as stacks of 16 bit TIFF files and analyzed with ImageJ software (http://rsb.info.nih.gov/ij/) or Metamorph software (Universal Imaging Corporation, West Chester, PA, USA).

Antibodies

The following primary antibodies were used: amphiphysins and endophilins kindly provided by Pietro Camilli, CIN85 (cat#231006 from Calbiochem, Darmstadt, Germany), PAK3 (cat#SC1871-N19 from Santa Cruz, CA, USA), OPHN1 (cat#SC8374-C19 Santa Cruz), GFP (cat#1814460 from Roche, Mannheim, Germany), Synaptophysin (cat#VAM-SV011 from StressGen, Canada), SNAP25 (cat#VAM-SV012 from StressGen, Canada), VGluT-1 kindly provided by S. El Mestikawy and B. Giros, GFAP (cat# sc-6170 from Santa Cruz), Tubulin (cat# T 6074 from Sigma), anti-MYPT1 antibody (cat#990407 from Upstate, NY, USA) and antiphospho-MYPT1 Thr853 (cat#36-003 from Upstate), GluR1 (Oncogene Research Products, Cambridge, MA, USA) or GluR2 (Chemicon International, Temecula, CA, USA). Fluorescent-conjugated secondary antibodies were purchased from Jackson Immuno-Research Labs, (West Grove, USA).

Electrophysiology

Mice were anaesthetized by intraperitoneal injection of a mixture of medetomide (1 mg/kg) and ketamine (76 mg/kg) prior to being killed by cervical dislocation, their brains removed for preparation of 400 µm ventral slices of the dorsal hippocampus slices using a Vibroslice (Campden Instruments, Loughborough, UK). Slices were placed in an interface recording chamber perfused with aCSF containing

(in mM): 125 NaCl, 26 NaHCO$_3$, 1.25 NaH$_2$PO$_4$, 3 KCl, 2 CaCl$_2$, 1 MgCl$_2$ and 10 Glucose, pH 7.4., gassed with 95% O$_2$, 5% CO$_2$, maintained at 32°C. Slices were allowed to recover for a period of 1 h prior to recording.

Stimuli were applied through a concentric stimulating electrode (Harvard Apparatus, Edenbridge, UK) placed in the stratum radiatum ∼150 µm from the CA1 pyramidal cell layer. Recordings of PSP were made from the same layer of stratum radiatum, ∼2 mm away, using glass microelectrodes, an Neurolog DC amplifier and a 1401plus signal acquisition system running Signal version 3.10 (Cambridge Electronic Design, Cambridge, UK). Stimulus response curves used a fixed set of stimulus strengths and the field PSPs were measured as the slope (between 20 and 80% of maximum. LTD was induced by 900 stimuli delivered at 1 Hz after at least 15 min of recording half maximal stimuli delivered every 60 s. The same test stimuli were then delivered for a further 45 min.

Statistical analyses

Microsoft Excel (Microsoft) with StatEL plugin from AdScience (France) was used for statistical analyses. All results are given as mean $\pm$ SEM unless otherwise stated. All probability values are given for an alpha level of 5% using MW as non-parametric test or two-tailed, unpaired Student's *t*-tests for analyses of data from synaptosomes.

SUPPLEMENTARY MATERIAL

Supplementary Material is available at *HMG* online.

ACKNOWLEDGEMENTS

Conflict of Interest statement. None declared.

FUNDING

REFERENCES

1. Chiurazzi, P., Schwartz, C.E., Gecz, J. and Neri, G. (2008) *XLMR* genes: update 2007. *Eur. J. Hum. Genet.*, **16**, 422–434.
2. Chelly, J., Khelfaoui, M., Francis, F., Cherif, B. and Bienvenu, T. (2006) Genetics and pathophysiology of mental retardation. *Eur. J. Hum. Genet.*, **14**, 701–713.
3. Billuart, P., Bienvenu, T., Ronce, N., des Portes, V., Vinet, M.C., Zemni, R., Roest Crollius, H., Carrie, A., Fauchereau, F., Cherry, M. *et al.* (1998) Oligophrenin-1 encodes a rhoGAP protein involved in X-linked mental retardation. *Nature*, **392**, 923–926.
4. des Portes, V., Boddaert, N., Sacco, S., Briault, S., Maincent, K., Bahi, N., Gomot, M., Ronce, N., Bursztyn, J., Adamsbaum, C. *et al.* (2004) Specific clinical and brain MRI features in mentally retarded patients with mutations in the Oligophrenin-1 gene. *Am. J. Med. Genet.*, **124**, 364–371.
5. Philip, N., Chabrol, B., Lossi, A.M., Cardoso, C., Guerrini, R., Dobyns, W.B., Raybaud, C. and Villard, L. (2003) Mutations in the oligophrenin-1 gene (*OPHN1*) cause X linked congenital cerebellar hypoplasia. *J. Med. Genet.*, **40**, 441–446.
6. Zanni, G., Saillour, Y., Nagara, M., Billuart, P., Castelnau, L., Moraine, C., Faivre, L., Bertini, E., Durr, A., Guichet, A. *et al.* (2005) Oligophrenin 1 mutations frequently cause X-linked mental retardation with cerebellar hypoplasia. *Neurology*, **65**, 1364–1369.
7. Khelfaoui, M., Denis, C., van Galen, E., de Bock, F., Schmitt, A., Houbron, C., Morice, E., Giros, B., Ramakers, G., Fagni, L. *et al.* (2007) Loss of X-linked mental retardation gene oligophrenin1 in mice impairs spatial memory and leads to ventricular enlargement and dendritic spine immaturity. *J. Neurosci.*, **27**, 9439–9450.
8. Chechlacz, M. and Gleeson, J.G. (2003) Is mental retardation a defect of synapse structure and function? *Pediatr. Neurol.*, **29**, 11–17.
9. Fiala, J.C., Spacek, J. and Harris, K.M. (2002) Dendritic spine pathology: cause or consequence of neurological disorders? *Brain Res. Brain Res. Rev.*, **39**, 29–54.
10. Peter, B.J., Kent, H.M., Mills, I.G., Vallis, Y., Butler, P.J., Evans, P.R. and McMahon, H.T. (2004) BAR domains as sensors of membrane curvature: the amphiphysin BAR structure. *Science*, **303**, 495–499.
11. Fauchereau, F., Herbrand, U., Chafey, P., Eberth, A., Koulakoff, A., Vinet, M.C., Ahmadian, M.R., Chelly, J. and Billuart, P. (2003) The RhoGAP activity of OPHN1, a new F-actin-binding protein, is negatively controlled by its amino-terminal domain. *Mol. Cell. Neurosci.*, **23**, 574–586.
12. Lichte, B., Veh, R.W., Meyer, H.E. and Kilimann, M.W. (1992) Amphiphysin, a novel protein associated with synaptic vesicles. *EMBO J.*, **11**, 2521–2530.
13. So, C.W., Caldas, C., Liu, M.M., Chen, S.J., Huang, Q.H., Gu, L.J., Sham, M.H., Wiedemann, L.M. and Chan, L.C. (1997) EEN encodes for a member of a new family of proteins containing an Src homology 3 domain and is the third gene located on chromosome 19p13 that fuses to MLL in human leukemia. *Proc. Natl Acad. Sci. USA*, **94**, 2563–2568.
14. Take, H., Watanabe, S., Takeda, K., Yu, Z.X., Iwata, N. and Kajigaya, S. (2000) Cloning and characterization of a novel adaptor protein, CIN85, that interacts with c-Cbl. *Biochem. Biophys. Res. Commun.*, **268**, 321–328.
15. David, C., McPherson, P.S., Mundigl, O. and de Camilli, P. (1996) A role of amphiphysin in synaptic vesicle endocytosis suggested by its binding to dynamin in nerve terminals. *Proc. Natl Acad. Sci. USA*, **93**, 331–335.
16. Dikic, I. (2003) Mechanisms controlling EGF receptor endocytosis and degradation. *Biochem. Soc. Trans.*, **31**, 1178–1181.
17. Sparks, A.B., Hoffman, N.G., McConnell, S.J., Fowlkes, D.M. and Kay, B.K. (1996) Cloning of ligand targets: systematic isolation of SH3 domain-containing proteins. *Nat. Biotech.*, **14**, 741–744.
18. Govek, E.E., Newey, S.E., Akerman, C.J., Cross, J.R., Van der Veken, L. and Van Aelst, L. (2004) The X-linked mental retardation protein oligophrenin-1 is required for dendritic spine morphogenesis. *Nat. Neurosci.*, **7**, 364–372.
19. Kawata, A., Iida, J., Ikeda, M., Sato, Y., Mori, H., Kansaku, A., Sumita, K., Fujiwara, N., Rokukawa, C., Hamano, M. *et al.* (2006) CIN85 is localized at synapses and forms a complex with S-SCAM via dendrin. *J. Biochem.*, **139**, 931–939.
20. De Gois, S., Jeanclos, E., Morris, M., Grewal, S., Varoqui, H. and Erickson, J.D. (2006) Identification of endophilins 1 and 3 as selective binding partners for VGLUT1 and their co-localization in neocortical glutamatergic synapses: implications for vesicular glutamate transporter

trafficking and excitatory vesicle formation. *Cell. Mol. Neurobiol.*, **26**, 679–693.

21. Ringstad, N., Gad, H., Low, P., Di Paolo, G., Brodin, L., Shupliakov, O. and De Camilli, P. (1999) Endophilin/SH3p4 is required for the transition from early to late stages in clathrin-mediated synaptic vesicle endocytosis. *Neuron*, **24**, 143–154.

22. Ringstad, N., Nemoto, Y. and De Camilli, P. (2001) Differential expression of endophilin 1 and 2 dimers at central nervous system synapses. *J. Biol. Chem.*, **276**, 40424–40430.

23. Manser, E., Loo, T.H., Koh, C.G., Zhao, Z.S., Chen, X.Q., Tan, L., Tan, I., Leung, T. and Lim, L. (1998) PAK kinases are directly coupled to the PIX family of nucleotide exchange factors. *Mol. Cell*, **1**, 183–192.

24. Cestra, G., Castagnoli, L., Dente, L., Minenkova, O., Petrelli, A., Migone, N., Hoffmuller, U., Schneider-Mergener, J. and Cesareni, G. (1999) The SH3 domains of endophilin and amphiphysin bind to the proline-rich region of synaptojanin 1 at distinct sites that display an unconventional binding specificity. *J. Biol. Chem.*, **274**, 32001–32007.

25. Kowanetz, K., Szymkiewicz, I., Haglund, K., Kowanetz, M., Husnjak, K., Taylor, J.D., Soubeyran, P., Engstrom, U., Ladbury, J.E. and Dikic, I. (2003) Identification of a novel proline-arginine motif involved in CIN85-dependent clustering of Cbl and down-regulation of epidermal growth factor receptors. *J. Biol. Chem.*, **278**, 39735–39746.

26. Kaneko, T., Maeda, A., Takefuji, M., Aoyama, H., Nakayama, M., Kawabata, S., Kawano, Y., Iwamatsu, A., Amano, M. and Kaibuchi, K. (2005) Rho mediates endocytosis of epidermal growth factor receptor through phosphorylation of endophilin A1 by Rho-kinase. *Genes Cells*, **10**, 973–987.

27. Lamaze, C., Chuang, T.H., Terlecky, L.J., Bokoch, G.M. and Schmid, S.L. (1996) Regulation of receptor-mediated endocytosis by Rho and Rac. *Nature*, **382**, 177–179.

28. Ito, M., Nakano, T., Erdodi, F. and Hartshorne, D.J. (2004) Myosin phosphatase: structure, regulation and function. *Mol. Cell. Biochem.*, **259**, 197–209.

29. Uehata, M., Ishizaki, T., Satoh, H., Ono, T., Kawahara, T., Morishita, T., Tamakawa, H., Yamagami, K., Inui, J., Maekawa, M. *et al.* (1997) Calcium sensitization of smooth muscle mediated by a Rho-associated protein kinase in hypertension. *Nature*, **389**, 990–994.

30. Malaval, C., Laffargue, M., Barbaras, R., Rolland, C., Peres, C., Champagne, E., Perret, B., Terce, F., Collet, X. and Martinez, L.O. (2009) RhoA/ROCK I signalling downstream of the P2Y13 ADP-receptor controls HDL endocytosis in human hepatocytes. *Cell. Signal.*, **21**, 120–127.

31. Di Paolo, G., Sankaranarayanan, S., Wenk, M.R., Daniell, L., Perucco, E., Caldarone, B.J., Flavell, R., Picciotto, M.R., Ryan, T.A., Cremona, O. *et al.* (2002) Decreased synaptic vesicle recycling efficiency and cognitive deficits in amphiphysin 1 knockout mice. *Neuron*, **33**, 789–804.

32. Marks, B. and McMahon, H.T. (1998) Calcium triggers calcineurin-dependent synaptic vesicle recycling in mammalian nerve terminals. *Curr. Biol.*, **8**, 740–749.

33. Cousin, M.A. and Robinson, P.J. (2000) Ca(2+) influx inhibits dynamin and arrests synaptic vesicle endocytosis at the active zone. *J. Neurosci.*, **20**, 949–957.

34. Ryan, T.A., Reuter, H., Wendland, B., Schweizer, F.E., Tsien, R.W. and Smith, S.J. (1993) The kinetics of synaptic vesicle recycling measured at single presynaptic boutons. *Neuron*, **11**, 713–724.

35. Takei, K., Mundigl, O., Daniell, L. and De Camilli, P. (1996) The synaptic vesicle cycle: a single vesicle budding step involving clathrin and dynamin. *J. Cell Biol.*, **133**, 1237–1250.

36. Man, H.Y., Lin, J.W., Ju, W.H., Ahmadian, G., Liu, L., Becker, L.E., Sheng, M. and Wang, Y.T. (2000) Regulation of AMPA receptor-mediated synaptic transmission by clathrin-dependent receptor internalization. *Neuron*, **25**, 649–662.

37. Holman, D., Feligioni, M. and Henley, J.M. (2007) Differential redistribution of native AMPA receptor complexes following LTD induction in acute hippocampal slices. *Neuropharmacology*, **52**, 92–99.

38. Yu, S.Y., Wu, D.C., Liu, L., Ge, Y. and Wang, Y.T. (2008) Role of AMPA receptor trafficking in NMDA receptor-dependent synaptic plasticity in the rat lateral amygdala. *J. Neurochem.*, **106**, 889–899.

39. Brown, T.C., Tran, I.C., Backos, D.S. and Esteban, J.A. (2005) NMDA receptor-dependent activation of the small GTPase Rab5 drives the removal of synaptic AMPA receptors during hippocampal LTD. *Neuron*, **45**, 81–94.

40. Lee, S.H., Liu, L., Wang, Y.T. and Sheng, M. (2002) Clathrin adaptor AP2 and NSF interact with overlapping sites of GluR2 and play distinct

roles in AMPA receptor trafficking and hippocampal LTD. *Neuron*, **36**, 661–674.

41. Eberth, A., Lundmark, R., Gremer, L., Dvorsky, R., Koessmeier, K.T., McMahon, H.T. and Ahmadian, M.R. (2008) A BAR domain-mediated autoinhibitory mechanism for RhoGAPs of the GRAF family. *Biochem. J.*, **417**, 371–377.

42. Srinivasan, G., Kim, J.H. and von Gersdorff, H. (2008) The pool of fast releasing vesicles is augmented by myosin light chain kinase inhibition at the calyx of Held synapse. *J. Neurophysiol.*, **99**, 1810–1824.

43. Voglmaier, S.M. and Edwards, R.H. (2007) Do different endocytic pathways make different synaptic vesicles? *Curr. Opin. Neurobiol.*, **17**, 374–380.

44. Granseth, B., Odermatt, B., Royle, S.J. and Lagnado, L. (2006) Clathrin-mediated endocytosis is the dominant mechanism of vesicle retrieval at hippocampal synapses. *Neuron*, **51**, 773–786.

45. Bianchi, V., Farisello, P., Baldelli, P., Meskenaite, V., Milanese, M., Vecellio, M., Muhlemann, S., Lipp, H.P., Bonanno, G., Benfenati, F. *et al.* (2009) Cognitive impairment in Gdi1-deficient mice is associated with altered synaptic vesicle pools and short-term synaptic plasticity, and can be corrected by appropriate learning training. *Hum. Mol. Genet.*, **18**, 105–117.

46. Chowdhury, S., Shepherd, J.D., Okuno, H., Lyford, G., Petralia, R.S., Plath, N., Kuhl, D., Huganir, R.L. and Worley, P.F. (2006) Arc/Arg3.1 interacts with the endocytic machinery to regulate AMPA receptor trafficking. *Neuron*, **52**, 445–459.

47. Shepherd, J.D., Rumbaugh, G., Wu, J., Chowdhury, S., Plath, N., Kuhl, D., Huganir, R.L. and Worley, P.F. (2006) Arc/Arg3.1 mediates homeostatic synaptic scaling of AMPA receptors. *Neuron*, **52**, 475–484.

48. Wenthold, R.J., Petralia, R.S., Blahos, J. II and Niedzielski, A.S. (1996) Evidence for multiple AMPA receptor complexes in hippocampal CA1/CA2 neurons. *J. Neurosci.*, **16**, 1982–1989.

49. Collingridge, G.L., Isaac, J.T. and Wang, Y.T. (2004) Receptor trafficking and synaptic plasticity. *Nat. Rev.*, **5**, 952–962.

50. Rial Verde, E.M., Lee-Osbourne, J., Worley, P.F., Malinow, R. and Cline, H.T. (2006) Increased expression of the immediate-early gene arc/arg3.1 reduces AMPA receptor-mediated synaptic transmission. *Neuron*, **52**, 461–474.

51. Park, S., Park, J.M., Kim, S., Kim, J.A., Shepherd, J.D., Smith-Hicks, C.L., Chowdhury, S., Kaufmann, W., Kuhl, D., Ryazanov, A.G. *et al.* (2008) Elongation factor 2 and fragile X mental retardation protein control the dynamic translation of Arc/Arg3.1 essential for mGluR-LTD. *Neuron*, **59**, 70–83.

52. Waung, M.W., Pfeiffer, B.E., Nosyreva, E.D., Ronesi, J.A. and Huber, K.M. (2008) Rapid translation of Arc/Arg3.1 selectively mediates mGluR-dependent LTD through persistent increases in AMPAR endocytosis rate. *Neuron*, **59**, 84–97.

53. Hollenberg, S.M., Sternglanz, R., Cheng, P.F. and Weintraub, H. (1995) Identification of a new family of tissue-specific basic helix-loop-helix proteins with a two-hybrid system. *Mol. Cell. Biol.*, **15**, 3813–3822.

54. Chien, C.T., Bartel, P.L., Sternglanz, R. and Fields, S. (1991) The two-hybrid system: a method to identify and clone genes for proteins that interact with a protein of interest. *Proc. Natl Acad. Sci. USA*, **88**, 9578–9582.

55. Einarson, M.B. (2001) Detection of protein–protein interactions using the GST fusion protein pulldown technique. *Molecular Cloning: a Laboratory Manual*, 3rd edn. Cold Spring Harbor Laboratory Press, Vol. 18, pp. 55–59.

56. Bongiorno-Borbone, L., Onofri, F., Giovedi, S., Ferrari, R., Girault, J.A. and Benfenati, F. (2002) The translocation of focal adhesion kinase in brain synaptosomes is regulated by phosphorylation and actin assembly. *J. Neurochem.*, **81**, 1212–1222.

57. Dunkley, P.R., Jarvie, P.E., Heath, J.W., Kidd, G.J. and Rostas, J.A. (1986) A rapid method for isolation of synaptosomes on Percoll gradients. *Brain Res.*, **372**, 115–129.

58. Nicholls, D.G. and Sihra, T.S. (1986) Synaptosomes possess an exocytotic pool of glutamate. *Nature*, **321**, 772–773.

59. Mozhayeva, M.G., Sara, Y., Liu, X. and Kavalali, E.T. (2002) Development of vesicle pools during maturation of hippocampal synapses. *J. Neurosci.*, **22**, 654–665.

60. Qualmann, B. and Kelly, R.B. (2000) Syndapin isoforms participate in receptor-mediated endocytosis and actin organization. *J. Cell Biol.*, **148**, 1047–1062.